Available online at www.sciencedirect.com

ScienceDirect

Ceramics International 40 (2014) 191–198

CERAMICS INTERNATIONAL

www.elsevier.com/locate/ceramint

Porosity dependence of elastic modulus of porous Cr_3C_2 ceramics

Lei Zhang[a,b], Kewei Gao[a,*], Anastasia Elias[b], Ziqiang Dong[b], Weixing Chen[b,**]

[a]School of Materials Science and Engineering, University of Science and Technology Beijing, Beijing 100083, China
[b]Department of Chemical and Materials Engineering, University of Alberta, Edmonton, Alberta, Canada T6G 2G6

Received 28 March 2013; received in revised form 29 May 2013; accepted 30 May 2013
Available online 6 June 2013

Abstract

Porous chromium carbide (Cr_3C_2) ceramics exhibiting a uniform and accessible porous structure comprised of three-dimensional connected struts were synthesized using a reactive sintering method. The effect of sintering temperature on the resulting microstructure of the porous Cr_3C_2 was studied. Young's modulus of the porous carbides was measured by dynamic mechanical analysis (DMA), and a semi-empirical model $E = E_0(1-P/P_c)^{1/J}$ was developed (based on the generalized mixture rule (GMR)), to describe the porosity dependence of Young's modulus for this type of carbide. The constants $P_c = 0.8$ and $J = 0.355$ were determined by fitting the model to the measured values. The relationship between the micro-hardness of the material and the microstructure of the pores was also investigated.

Keywords: B. Porosity; DMA; Young's modulus; Micro-hardness; Cr_3C_2

1. Introduction

Macroporous ceramics (pore width > 50 nm) with a wide range of porosities have been extensively applied in environments involving corrosive media, extensive wear and high temperature [1]. Applications for these materials include catalyst carriers, gas separators, bioreactors, filters for hot corrosive gas and particulates in exhaust gas, thermal insulators and heat exchangers [2]. These applications take advantage of the attractive properties exhibited by porous materials at high-temperatures, including chemical stability, high permeability, low thermal conductivity, low weight and variable porosity. The main processes used to prepare macroporous ceramics include replica, sacrificial template and direct foaming techniques. In our study, macroporous chromium carbide (Cr_3C_2) with three-dimensional connected struts was synthesized using a reactive sintering method.

Cr_3C_2 is frequently used as the reinforcing phase in coating materials, owning to its high hardness (27 GPa [3]), and its excellent resistance to oxidation, erosion and wear. The synthesis of Cr_3C_2 can be generally classified as either direct or indirect. In direct synthesis, metal chromium is directly reacted with a carbon source at high temperature to yield Cr_3C_2 [4–6]. For example, Sharafi et al. have prepared nanocrystalline Cr_3C_2 powders using high energy milling to form a mixture of metal chromium and carbon powder, which was then compacted and sintered at 1100 °C [7]. Cr_3C_2 can be also synthesized as an interfacial coating by immersing carbon fibers into a Cu–Cr melt maintained at 1150 °C [8]. In indirect synthesis, Cr_3C_2 is formed by the reduction of chromium compounds. Chromium oxide (Cr_2O_3) is typically used as a chromium source, and is reduced by carbon in a carbothermical reduction process performed above 1200 °C [9,10]. It has also been shown that $(NH_4)_2Cr_2O_7$ can be also used as the chromium source; this material can be reduced with carbon at 1100 °C to form Cr_3C_2. Other sources of chromium have also been explored: in 1996 it was reported that $MgCr_2O_4$ could be carburized by carbon powder at 1450 °C to prepare bulk Cr_3C_2 [11]. $CrCl_3$ has been used to deposit whisker layers of Cr_3C_2 in a mixture gas containing C_4H_{10} at 900 °C [12]. To our knowledge, Cr_3C_2 synthesized through the reduction of Cr_2O_3 by methane has seldom been studied [13,14].

In this paper, porous Cr_3C_2 ceramics exhibiting a uniform and accessible porous structure with three-dimensional connected struts were synthesized by reducing Cr_2O_3 in methane. The

*Corresponding author. Tel./fax: +86 10 62334909.
**Corresponding author. Tel.: +1 780 492 7706; fax: +1 780 492 2881.
E-mail addresses: kwgao@yahoo.com, yroc_ustb@hotmail.com (K. Gao), weixing.chen@ualberta.ca (W. Chen).

0272-8842/$ - see front matter
http://dx.doi.org/10.1016/j.ceramint.2013.05.122

relationship between the temperature of the sintering reaction and the resulting microstructure of the porous Cr_3C_2 was studied. The elastic modulus of porous Cr_3C_2 was measured using dynamic mechanical analysis (DMA) [15,16]. The porosity dependence of Young's modulus of Cr_3C_2 was analyzed, and a new theoretical model based on the generalized mixture rule (GMR) was proposed to describe the elastic properties of the porous Cr_3C_2.

2. Experimental

2.1. Preparation of porous Cr_3C_2

Two reactive sintering processes were used to prepare the open-pore Cr_3C_2. In the first process, which is an indirect process, commercial chromium oxide (Cr_2O_3) powder (Alfa Aesar, USA, −325 mesh, purity of 98+%) and 10 wt% polyethylene glycol (PEG-400, Alfa Aesar) were mixed by ball milling in ethanol for 24 h. The mixed powders were then dried and uniaxially compressed in a cylindrical mold under a pressure of 80 MPa to form disc-shaped samples with diameters of 38 mm. The disc-shaped samples were pre-sintered at 150 °C for 1 h and then heated to 1000 °C for 2 h in a tube furnace (GSL 1200X, MTI Corporation). PEG was used as a porogen, and was burned off during the sintering process. The samples were subsequently sintered in the tube furnace at either 1000 °C, 1100 °C, 1200 °C or 1300 °C for 20 h. During the sintering process a carbonaceous gas mixture (10% CH_4, 40% Argon and 50% H_2 Praxair Canada) was flowed through the tube furnace at a rate of 60 ml/min, forming Cr_3C_2. A second process was also utilized to prepare samples with lower porosities. In the second process, commercial chromium carbide (Cr_3C_2, Alfa Aesar, USA, −325mesh, purity of 99.5%) was used as the starting material. This material was mixed with 10 wt% PEG, and the resulting powders were pressed to form disc-shape samples under the same pressure of 80 MPa. These samples were sintered in a tube furnace (GSL 1600X, MTI Corporation) at 1100 °C for 20 h, while a carbonaceous gas mixture (10% CH_4, 40% Argon and 50% H_2, Praxair Canada) was flowed over the sample at 10 ml/min.

2.2. Sample characterization

The morphologies of the samples were examined by field emission scanning electron microscopy (FE-SEM, Zeiss, EVO-MA15). Both surface and cross-sectional images were obtained. To obtain cross-sectional images, samples were cleaved by breaking the as-synthesized Cr_3C_2 samples into two pieces by holding the samples with two sets of tweezers and applying a flexural force. The porous properties of as-carbonized samples were characterized using a mercury intrusion porosimeter (AutoPore IV 9510). To obtain Young's modulus of the materials, rectangular samples with dimensions of 35 mm × 8 mm × 1 mm were cut from the disks, and their surfaces were polished with a #400 grinding paper. Samples were then tested by dynamic mechanical analysis (DMA 8000, Perkin-Elmer) at 1 Hz and room temperature to a displacement of 0.01 mm using the three point-bending mode. The hardness of the porous ceramics was measured using a micro-indentation hardness tester (Buehler, USA, IndentaMet 1100 Series), with a load of 100 g.

3. Results and discussion

3.1. Microstructure

Figs. 1 and 2 show the surfaces and cross-sectional morphologies of as-synthesized Cr_3C_2 samples respectively,

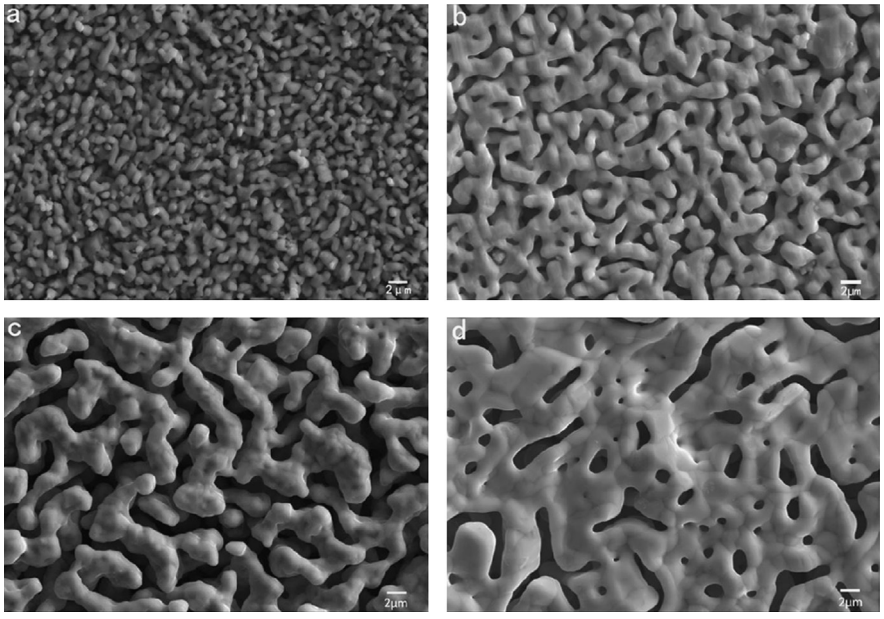

Fig. 1. Surface morphologies of porous Cr_3C_2 samples carbonized from Cr_2O_3 for 20 h at (a) 1000 °C; (b) 1100 °C; (c) 1200 °C; and (d) 1300 °C.

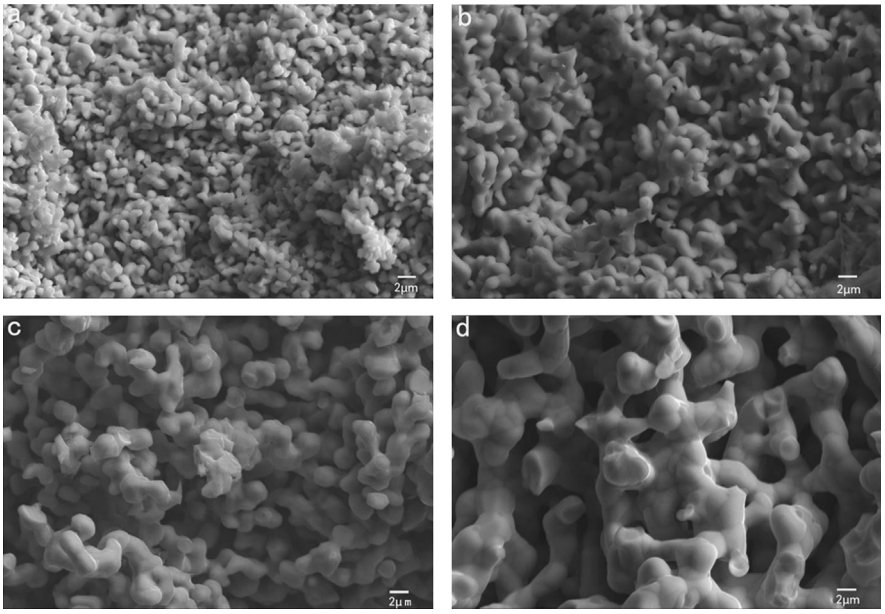

Fig. 2. Cross-section morphologies of porous Cr_3C_2 samples carbonized from Cr_2O_3 at different temperatures for 20 h: (a) 1000 °C; (b) 1100 °C; (c) 1200 °C; and (d) 1300 °C.

prepared using the first process (in which Cr is supplied by Cr_2O_3 powder), for samples sintered at 1000 °C, 1100 °C, 1200 °C and 1300 °C. A dense network of open pores covers the surface of the samples, as shown in Fig. 1, and a continuous structure of pores is distributed throughout the interior, as shown in Fig. 2. The average sizes of both the pores and strut increase with the increasing sintering temperature. The continuous structure of pores forms gradually during the sintering process as Cr_2O_3 is gradually transformed to Cr_3C_2. Due to the high diffusivity of chromium and oxygen atoms at the high temperatures utilized during sintering [17], small particles combine together to form larger particles, and ultimately struts. As diffusion is a temperature dependent process, larger structures form at higher temperatures, leaving higher voids or pores.

The surface and cross-sectional morphologies of the samples prepared from Cr_3C_2 and PEG at 1100 °C using the second process (which uses Cr_3C_2 as the starting material) are shown in Fig. 3. These samples have similar microstructure with those prepared by the first process (from Cr_2O_3) at 1100 °C, but different densities. The lower density attained can mainly be attributed to the lower density of the initial mixture of Cr_3C_2 and PEG.

The mechanism by which chromium carbide is formed through the carbothermal reduction of chromium oxide in the gas mixture utilized here (10% CH_4+40% Ar+H_2 (balance)) has been studied in detail previously by our group [18–20]. This environment has a very high carbon activity. It was experimentally confirmed that the chromium oxide phase is first converted to Cr_7C_3 and then to Cr_3C_2, which is the most stable form of chromium carbides. The final reaction can be expressed as

$$Cr_2O_3(s) + \frac{13}{3}CH_4(s) \rightarrow \frac{2}{3}Cr_3C_2(s) + 3CO(g) + \frac{26}{3}H_2(g) \qquad (1)$$

A porous carbide with a continuous network of pores is produced during this process, and is believed to result from a combination of the following two processes: (1) the coalescence of the original pores in the as-pressed chromium oxide samples during the sintering process; and (2) the volume reduction due to the phase transformation from Cr_2O_3 to Cr_3C_2. The formation of the pores further allows the carbonaceous reducing gas to access the interior chromium oxide particles in the sample, producing a uniform network of pores throughout.

3.2. Physical characterization

The porosity of porous carbide ceramics was determined from the following equation:

$$p = 1 - \frac{m/\rho_0}{V} \qquad (2)$$

where ρ_0 is the bulk density of the equivalent solid matrix material (without pores), which is 6.68 g cm^{-3} for Cr_3C_2 [3], and m and V are the mass and the volume of the bulk porous material, respectively. Fig. 4 shows the calculated results of the porosity of porous chromium carbides carbonized from Cr_2O_3/PEG mixtures at different temperatures. Each data point was obtained from six different samples sintered at the same temperature. Average values and standard deviations are shown. It can be seen that average porosities of 58%, 64%, 60% and 57% were achieved at sintering temperatures of 1000 °C, 1100 °C, 1200 °C and 1300 °C, respectively. The porosity of the porous carbide decreased slightly when the carbonization temperature was increased above 1100 °C. Therefore, it seems that the carbonization temperature has only a weak influence on the porosity of porous carbide obtained. The initial porosity of the as-pressed Cr_2O_3 samples was measured to be between 45% and 50% (determined by Eq. (2) using ρ_0=5.22 g cm^{-3} for Cr_2O_3 [21] and m=90 wt% total mass, since 10% of the initial mass was PEG), so it can be

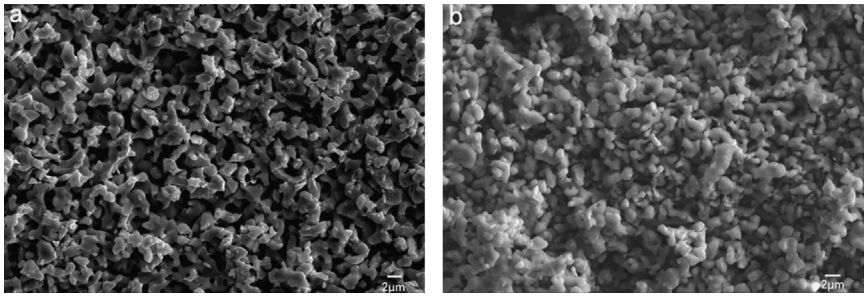

Fig. 3. SEM images of porous Cr_3C_2 samples prepared from Cr_3C_2 and PEG by the second process (using Cr_3C_2 as the starting material) seen from (a) the surface; and (b) in cross-section.

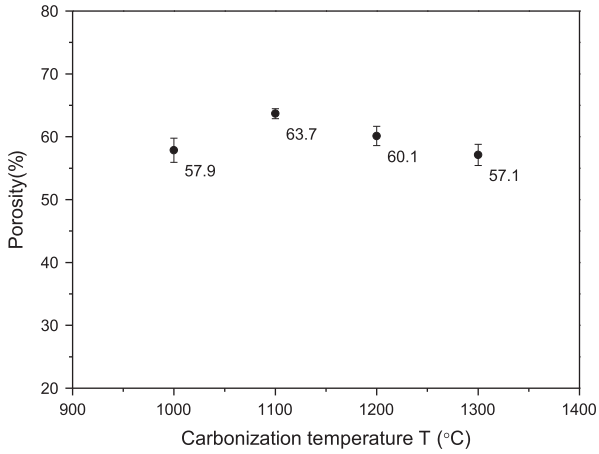

Fig. 4. Total porosity of porous Cr_3C_2 for various carbonization temperatures. Average values and standard deviations from six samples per data point are shown.

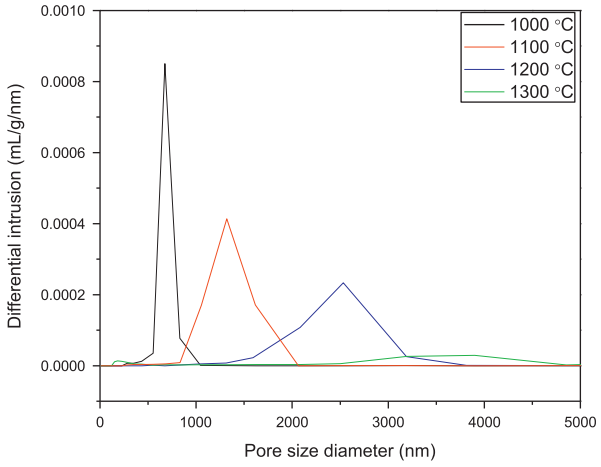

Fig. 5. The distribution of pore diameter of the porous Cr_3C_2 samples carbonized from different temperatures.

calculated that the volume reduction due to the phase transformation from Cr_2O_3 to Cr_3C_2 in the reaction sintering process is about 10–15% (relatively independent of the carbonization temperature). We expect that the slight decrease in volume fraction of the material that occurs at sintering temperatures above 1100 °C occurs due to an increase in the density of the grains in Cr_3C_2.

The distribution of the pore diameters of the porous Cr_3C_2 samples is shown in Fig. 5, as measured by mercury intrusion porosimetry, which is an effective method for characterizing the properties of porous materials [22]. It can be seen that for the porous samples synthesized from Cr_2O_3/PEG mixtures, the average pore size increases from 0.8 μm to 3.5 μm as the carbonization temperature increases from 1000 °C to 1300 °C. Similarly, the distribution of the pore diameters increases strongly as the sintering temperature increases. Table 1 summarizes the physical characteristics of the porous Cr_3C_2 formed by carbonization at different temperatures via mercury intrusion porosimetry. The data is consistent with the quantitative observations made from the SEM images, which showed that both larger pores and larger struts evolved at higher temperatures. This corresponds to a decrease in specific surface area. The process is strongly affected by the sintering temperature and holding time. At higher temperatures, diffusion is enhanced, and larger pores and struts result. The small differences between the porosities calculated from the sample mass, volume and density and the values obtained using mercury intrusion porosimetry can be attributed to the fact that mercury intrusion porosimetry does not effectively measure the volume of trapped pores, which are found in our samples.

3.3. Porosity dependence of Young' modulus

Young's modulus is a key mechanical property of isotropic brittle materials such as ceramics [23]. It is correlated with most mechanical properties including hardness, tensile strength, bending strength, fracture toughness, and so on. Young's modulus of the open-pore Cr_3C_2 was measured by dynamic mechanical analysis in the three-point bending mode, and the relationship between Young's modulus and porosity was fitted using the OriginPro 8.5 software, as shown in Fig. 6.

The dependence of the mechanical properties of ceramics on type, size, distribution and volume fraction of pores has been extensively studied over the past 30 years [25–36]. Many efforts have been made to model the dependence of mechanical properties on the porosity of engineering ceramics. Based on experimental results, a number of models have been proposed to represent the relationship between mechanical properties and porosity. The most frequently employed

equations describing the mechanical behavior of porous ceramics are listed in Table 2.

Eqs. (3)–(6) are semi-empirical models derived from fitting experimental results of specific type of porous ceramics. Hence, these equations have some limitations. They typically only describe a limited range of porosities, and cannot be applied to all polycrystalline brittle solids, because the effects of pore type, size and distribution are not considered in these equations. To resolve the problem, Eq. (8) was derived by Phani and Niyogi to predict Young's modulus of polycrystalline ceramics over a wide range of porosities. This equation was built on the assumption that the pore distribution, size and shape are random. The constant a in Eq. (8) is defined as a "packing geometry factor" which is related to the critical porosity $P_c = 1/a$, at which the elastic modulus of porous ceramics becomes zero. Another constant f depends on the pore geometry and the strut morphology. When the critical porosity $P_c = 1/a$ is equal to 1, Eq. (8) can be simplified to Eq. (7).

S. Ji et al. [35,36] proposed a unified model (Eq. (9)) named the Generalized Mixture Rule (GMR) to describe the porosity dependence of mechanical properties of multi-phases solid materials. In this equation, a fractal parameter J represents the effect of the shape, size, and distribution of each phase on the mechanical properties of the composite. Eq. (10) is a simplified expression of GMR for porous brittle solids, which are considered a special class of two-phase composites in which null strength pores are dispersed within a solid framework. Eq. (10) can be expressed in the form of a power series, as shown in the following equation:

$$\frac{M_c}{M_s} = 1 + \left(-\frac{1}{J}P\right) + \frac{(1/J)((1/J)-1)}{2}P^2 + \frac{-(1/J)((1/J)-1)((1/J)-2)}{6}P^3 + \cdots \quad (11)$$

where the subscripts c and s refer to the composite and the strengthened phases, respectively. Eq. (11) can also be converted to Eqs. (3)–(5), when the porosity is low ($P \ll 1$) in some specific situations. In a porous ceramic, the pores themselves are considered to be a phase whose mechanical properties are equal to zero. The GMR model has been found to be valid to simulate the mechanical properties of a wide range of composites and porous ceramics [36]. However, it is not suitable to calculate the mechanical properties of porous materials with a high volume fraction of pores, in which case the engineering mechanical strength of the porous material tend toward zero. Therefore, a modified GMR Eq. (12) was proposed based on the experimental data obtained from our study, aiming to predict the mechanical properties of highly porous ceramics. The modified GMR equation is stated in the

Table 1
The properties of porous carbide pre-forms carbonized at different temperatures for 20 h.

Carbonization temperature (°C)	1000	1100	1200	1300
Average pore diameter (μm)	0.8	1.3	2.5	3.5
Total surface area ($m^2\ g^{-1}$)	0.798	0.677	0.357	0.127
Nominal density ($g\ cm^{-3}$)	2.94	2.38	2.31	2.33
Porosity (%)	56.9	60.1	55.1	47.2

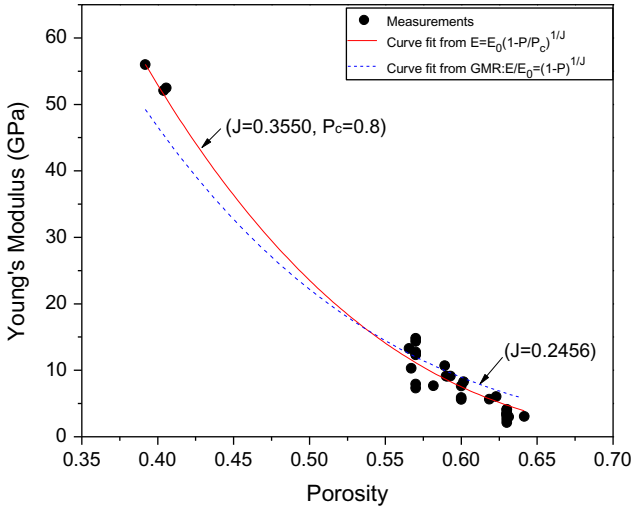

Fig. 6. Curve fitting the porosity dependence of Young's modulus in the continuous open pore Cr_3C_2.

Table 2
Semi-empirical formulae describing Young's modulus as a function of volume fraction porosity P. M is an elastic property (such as modulus, hardness, etc.) and E is the Young modulus. The values of h, f, b, A, P_c and J are determined by fitting the formulae to experimental results.

Author (year)	Reference	Equation	
	[24,25]	$E = E_0(1-hP)$	(3)
Ryshkewitch–Duckworth (1953)	[26–28]	$E = E_0\exp(-bP)$	(4)
Knudsen (1959)	[25,29]	$E = E_0(1-f_1P+f_2P^2)$	(5)
Hasselman (1962)	[30,31]	$E = E_0\left\{1+\frac{AP}{[1-(A+1)P]}\right\}$	(6)
Phani–Niyogi (1987)	[32,33]	$E = E_0(1-P)^n$	(7)
Phani–Niyogi (1987)	[25,32,34]	$E = E_0(1-aP)^f$	(8)
Shaocheng Ji (2004)	[35,36]	$M_c^J = \sum_i^N (V_i M_i^J)$	(9)
		$\frac{M_c}{M_s} = (1-P)^{1/J}$	(10)

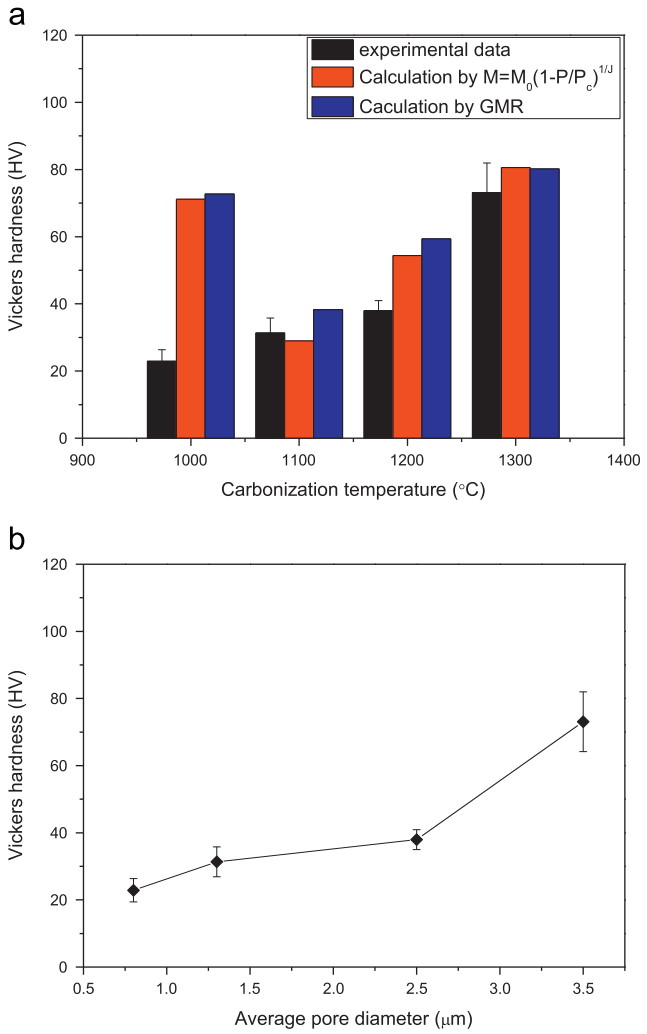

Fig. 7. (a) Micro-hardness of the porous chromium carbides carbonized at different temperatures. Average values and mean squared-error values are shown for measurements on 10 samples. (b) Micro-hardness of the porous chromium carbides with different average pore diameters. Average values and standard deviations from 10 samples are shown.

following equation:

$$E = E_0\left(1-\frac{P}{P_c}\right)^{1/J} \tag{12}$$

This equation is very similar to Eq. (8), however the volume fraction porosity P is scaled against the critical porosity P_c, enabling a more accurate picture of the material to be captured at high porosities. The correlation of Young's modulus with the porosity of the carbide is shown in Fig. 6. In order to obtain a wide range porosity of porous carbide, the second reaction sintering process was employed to prepare the samples from Cr_3C_2/PEG with porosities around 40%. It can be seen that Young's modulus of carbide drops sharply when the porosity of carbide increases from 40% to 65%. As shown in Fig. 6, the fitting curve employed by the GMR model does not agree well with all of the data points. The deviation of the GMR fitting curve from the experimental results may result from the existence of a critical porosity P_c, at which Young's modulus of the open-pore ceramic approaches zero [37,38]. Fig. 6 also shows the fitting curve based on the modified model (Eq. (12)) ($E_0 = 380$ GPa for Cr_3C_2), which can accurately fit all the data obtained, using the parameters $P_c = 0.8$ and $J = 0.355$.

Physically, P_c has been proposed to be the initial porosity $(1-\rho_0)$ of porous materials prepared by a powder sintering process, where ρ_0 is the "initial relative density" [39]. In our carbides, P_c does not match the measured values of the initial porosity (between 0.45 and 0.5). This discrepancy may be attributed to the specific method in which the phase transformation occurred in our process. The exponent J is considered to depend on the geometrical shape, spatial arrangement, orientation and size distribution of pores, and its value should lie in the range from 0 to 1. $J = 1$ for porous materials with long cylindrical or hexagonal pores aligned parallel to the direction of stress, and $J = 0$ represents an extreme case where the effective mechanical properties of a porous material will become zero regardless of porosity. Generally, intergranular, continuous, channel pores cavities are characterized by a lower J value than intragranular, isolated and rounded pores. The open pores exhibit a lower J value and thus have a more pronounced effect on the effective mechanical properties than the closed pores. As the porous Cr_3C_2 studied in this paper has been determined by SEM and porosimetry to be comprised of intergranular, continuous and channel-like pore cavities structures, a low value of J is expected. The value $J = 0.355$ which was fitted from experimental data is consistent well with the semi-empirical laws.

3.4. Hardness

Hardness is an important parameter describing the resistance of a material to plastic deformation. This property is intimately related to other mechanical properties such as bending strength, wear resistance, compressibility, toughness, elastic modulus and so on [40]. The hardness of porous ceramics is also strongly influenced by porosity. Here, the hardness of porous Cr_3C_2 samples prepared from Cr_2O_3/PEG was measured by indentation hardness testing. The measured values of Vickers hardness (HV) of different porous samples are shown in Fig. 7, and are compared with the values calculated using two different models. The measured Vickers hardness (M) increased from about 22.9 to about 73.1 as the carbonization temperature increased from 1000 °C to 1300 °C. At all temperature points other than 1000 °C, the measured values matched well with the theoretical values calculated by our model $M = M_0(1-P/P_c)^{1/J}$ (with fitted constants $P_c = 0.8$ and $J = 0.355$). It also can be seen that the measurement Vickers hardness increased as the average pore size increased from 0.8 μm to 3.5 μm in Fig. 6(b). As we observed previously, the reaction sintering temperature has a strong influence on the size, shape and distribution of the grains. We conclude that the hardness of the porous chromium is also strongly influenced by pore structure, which is highly dependent on sintering temperature.

4. Conclusions

Porous Cr_3C_2 with a continuous open pore structure was fabricated by a reaction sintering process. The porosities of carbides carbonized from Cr_2O_3 are concentrated in a narrow range of 55–65% for sintering temperatures between 1000 °C and 1300 °C. As the carbonization temperature increased from 1000 °C to 1300 °C, the average pore size increased from 0.8 μm to 3.5 μm, while the distribution of the pore diameters became more dispersed.

The porosity of the carbides is mainly attributed to two factors: (1) the initial gaps and binding materials between packed chromium oxide powders (with −325 mesh particle size) mixed with 10% PEG under 80 MPa pressure (45–55%); and (2) the volume reduction of the phase transformation from Cr_2O_3 to Cr_3C_2 (approximately 10–15% of the initial volume). The sintering temperature contributed only weakly to the overall porosity of porous Cr_3C_2, despite the differences in pore size and distribution observed at different temperatures.

Young's modulus of the porous Cr_3C_2 decreased rapidly as the porosity increased. A semi-empirical equation $E = E_0(1-P/P_c)^{1/J}$ was developed from the GMR to describe the porosity dependence of Young's modulus in the continuous open pore carbides, and a group of constants, $P_c=0.8$, and $J=0.355$, were fit from the experimental data. These constants are helpful in evaluating the mechanical properties of porous Cr_3C_2 with similar microstructures and investigating the relationship between mechanical properties with porosity in porous materials.

The hardness of the porous Cr_3C_2 is mainly affected by the pore structure. The value of Vickers hardness varied from 20 to 90 as the average pore size increased from 0.8 μm to 3.5 μm.

Acknowledgment

The authors would like to acknowledge the financial support by Natural Sciences and Engineering Research Council of Canada (NSERC) and China Scholarship Council (CSC).

References

[1] A.R. Studart, U.T. Gonzenbach, E. Tervoort, L.J. Gauckler, Processing routes to macroporous ceramics: a review, Journal of the American Ceramic Society 89 (2006) 1771–1789.
[2] L. Shi, H. Zhao, Y. Yan, Z. Li, C. Tang, Porous titanium carbide ceramics fabricated by coat-mix process, Scripta Materialia 55 (2006) 763–765.
[3] R. Riedel, Handbook of Ceramic Hard Materials, 2000, p. 203.
[4] P. Matteazzi, G. Lecaer, Room-temperature mechanosynthesis of carbides by grinding of elemental powders, Journal of the American Ceramic Society 74 (1991) 1382–1390.
[5] H. Huang, P.G. McCormick, Effect of milling conditions on the synthesis of chromium carbides by mechanical alloying, Journal of Alloys and Compounds 256 (1997) 258–262.
[6] A. Kunrath, K. Upadhya, I. Reimanis, J. Moore, Synthesis and application of composite TIC–Cr_3C_2 targets, Surface and Coatings Technology 94 (1997) 237–241.
[7] S. Sharafi, S. Gomari, Effects of milling and subsequent consolidation treatment on the microstructural properties and hardness of the nanocrystalline chromium carbide powders, International Journal of Refractory Metals and Hard Materials 30 (2012) 57–63.
[8] D. Himbeault, R. Varin, K. Piekarski, Carbon fibers coated with chromium carbide using the liquid metal transfer agent technique, Metallurgical and Materials Transactions A 20 (1989) 165–170.
[9] P. Rajagopalan, T. Krishnan, D. Bose, Development of carbothermy for the preparation of hepta chromium carbide, Journal of Alloys and Compounds 297 (2000) L1–L4.
[10] L.M. Berger, S. Stolle, W. Gruner, K. Wetzig, Investigation of the carbothermal reduction process of chromium oxide by micro- and lab-scale methods, International Journal of Refractory Metals and Hard Materials 19 (2001) 109–121.
[11] S. Hashimoto, A. Yamaguchi, Preparation of porous Cr_3C_2 grains with Cr_2O_3, Journal of the American Ceramic Society 79 (1996) 2503–2505.
[12] S. Motojima, S. Kuzuya, Deposition and whisker growth of Cr_3C_2 by CVD process, Journal of Crystal Growth 71 (1985) 682–688.
[13] R. Ebrahimi-Kahrizsangi, H.M. Zadeh, V. Nemati, Synthesis of chromium carbide by reduction of chromium oxide with methane, International Journal of Refractory Metals and Hard Materials 28 (2010) 412–415.
[14] T.Y. Xing, X.W. Cui, W.X. Chen, R.S. Yang, Synthesis of porous chromium carbides by carburization, Materials Chemistry and Physics 128 (2011) 181–186.
[15] L.F.C.P. Lima, A.L.E. Godoy, E.N.S. Muccillo, Elastic modulus of porous Ce-TZP ceramics, Materials Letters 58 (2004) 172–175.
[16] G. Swaminathan, K.N. Shivakumar, L.C. Russell, Anomalies, influencing factors, and guidelines for DMA testing of fiber reinforced composites, Polymer Composites 30 (2009) 962–969.
[17] M.W. Barsoum, Fundamentals of Ceramics, Mcgraw-Hill Companies, New York, 1997, p. 40.
[18] H. Li, Y.J. Zheng, L.W. Benum, M. Oballa, W.X. Chen, Carburization behaviour of Mn–Cr–O spinel in high temperature hydrocarbon cracking environment, Corrosion Science 51 (2009) 2336–2341.
[19] H. Li, W.X. Chen, Stability of $MnCr_2O_4$ spinel and Cr_2O_3 in high temperature carbonaceous environments with varied oxygen partial pressures, Corrosion Science 52 (2010) 2481–2488.
[20] H. Li, X.W. Cui, W.X. Chen, Effect of CeO_2 on high temperature carburization behavior of Mn–Cr–O spinel and chromium oxide, Journal of the Electrochemical Society 157 (2010) C321–C327.
[21] J.F. Shackelford, W. Alexander, CRC Materials Science and Engineering Handbook, 2000, pp. 20–52.
[22] J. Rouquerol, et al., The characterization of macroporous solids: an overview of the methodology, Microporous and Mesoporous Materials 154 (2012) 2–6.
[23] W. Pabst, E. Gregorova, G. Ticha, Elasticity of porous ceramics—a critical study of modulus–porosity relations, Journal of the European Ceramic Society 26 (2006) 1085–1097.
[24] E.A. Dean, J.A. Lopez, Empirical dependence of elastic-moduli on porosity for ceramic materials, Journal of the American Ceramic Society 66 (1983) 366–370.
[25] K.K. Phani, S.K. Niyogi, Elastic-modulus porosity relationship for Si_3N_4, Journal of Materials Science Letters 6 (1987) 511–515.
[26] E. Ryshkewitch, Compression strength of porous sintered alumina and zirconia.9. To ceramography, Journal of the American Ceramic Society 36 (1953) 65–68.
[27] J.C. Wang, Young modulus of porous materials.1. Theoretical derivation of modulus porosity correlation, Journal of Materials Science 19 (1984) 801–808.
[28] V.D. Krstic, W.H. Erickson, A model for the porosity dependence of Young modulus in brittle solids based on crack opening displacement, Journal of Materials Science 22 (1987) 2881–2886.
[29] K.K. Phani, S.K. Niyogi, Porosity dependence of ultrasonic velocity and elastic-modulus in sintered uranium-dioxide—a discussion, Journal of Materials Science Letters 5 (1986) 427–430.
[30] D.P.H. Hasselman, On the porosity dependence of the elastic moduli of polycrystalline refractory materials, Journal of the American Ceramic Society 45 (1962) 452–453.

[31] K.K. Phani, Elastic-constant–porosity relations for polycrystalline thoria, Journal of Materials Science Letters 5 (1986) 747–750.
[32] K.K. Phani, S.K. Niyogi, Young modulus of porous brittle solids, Journal of Materials Science 22 (1987) 257–263.
[33] A.S. Wagh, R.B. Poeppel, J.P. Singh, Open pore description of mechanical-properties of ceramics, Journal of Materials Science 26 (1991) 3862–3868.
[34] K.K. Phani, S.K. Niyogi, A.K. De, Porosity dependence of fracture mechanical-properties of reaction sintered Si_3N_4, Journal of Materials Science Letters 7 (1988) 1253–1256.
[35] S.C. Ji, Generalized means as an approach for predicting Young's moduli of multiphase materials, Materials Science and Engineering A—Structural Materials Properties Microstructure and Processing 366 (2004) 195–201.
[36] S.C. Ji, Q. Gu, B. Xia, Porosity dependence of mechanical properties of solid materials, Journal of Materials Science 41 (2006) 1757–1768.
[37] J. Kovacik, Correlation between shear modulus and porosity in porous materials, Journal of Materials Science Letters 20 (2001) 1953–1955.
[38] J. Kovacik, Correlation between elastic modulus, shear modulus, Poisson's ratio and porosity in porous materials, Advanced Engineering Materials 10 (2008) 250–252.
[39] D.C.C. Lam, F.F. Lange, A.G. Evans, Mechanical-properties of partially dense alumina produced from powder compacts, Journal of the American Ceramic Society 77 (1994) 2113–2117.
[40] J. Luo, R. Stevens, Porosity-dependence of elastic moduli and hardness of 3Y-TZP ceramics, Ceramics International 25 (1999) 281–286.